Intrapulse x-ray parametric amplification in high-order-harmonic generation

Carles Serrat*
Universitat Politècnica de Catalunya, Colom 11, 08222 Terrassa, Barcelona, Spain
(Received 20 April 2016; published xxxxxx)

We demonstrate strong-field-driven impulsive XUV–x-ray parametric amplification (IXPA) processes in high-order harmonic generation at the single-atom level by using *ab initio* calculations. We consider the example of Li^+ ions exposed simultaneously to an intense IR pulse and a weak 200-as XUV–x-ray pulse with central photon energies varying from 90 to 400 eV. We determine optimal parameter ranges and the precise delays between the IR and the XUV–x-ray pulses for IXPA to occur. The present results might be a guide to achieve exponential growth of the XUV–x-ray signal in tabletop XUV–x-ray lasers.

DOI: 10.1103/PhysRevA.00.003400

Extreme ultraviolet (XUV) and x-ray coherent ultrashort light pulses can be generated in tabletop high-order harmonic generation (HHG) sources. Important applications suffer, however, from the low efficiency inherent to HHG processes. Different techniques have been investigated to overcome this low efficiency and important advances have been made [1–8]. Strong-field assisted XUV–x-ray parametric amplification processes in particular are investigated since they can produce avalanche effects in the medium that result in an exponential growth of the XUV–x-ray signal [9–15].

In previous research we addressed the influence of weak XUV radiation pulses of photon energies far from the ionization potential of the medium added to the strong IR driving pulse in HHG processes [11,13,14,16,17]. In particular, we showed that forward scattering can be largely enhanced when an XUV pulse is optimally synchronized with the IR pulse [11]. This theoretical prediction was soon corroborated by experiments [12] and a further detailed comparison between the theory and the experimental measurements showed good qualitative agreement [14]. Strong-field-mediated intrapulse x-ray parametric amplification (IXPA) processes were identified in [14] as decisive for the amplification at the single-atom level. The theory used in these previous studies was based on the strong-field approximation (SFA) [18]. It is therefore important to investigate the effect of the Coulomb potential of the atom, which is basically neglected in the SFA, on the amplification effects.

In this paper we perform time-dependent Schrödinger equation (TDSE) simulations in one dimension [19–21], which correctly consider the effect of the Coulomb potential, and demonstrate the IXPA effect using an *ab initio* theory by considering the Li^+ ion ($I_p = 75.6$ eV) as the amplifying medium. We have chosen to investigate optimal parameter ranges for IXPA in Li^+ for two reasons. First, parametric XUV–x-ray amplification effects were shown to benefit at the single-atom level by high gas ionization potentials [13]. Harmonics with large contrast were predicted compared to the broad spectrum obtained from the lower ionization potentials of gases as He. Second, a high ionization potential will also favor the avalanche effect produced by the parametric amplification processes [14], because those need a high degree of synchronization between the XUV–x-ray and IR pulses, and this synchronization is optimally preserved by the lower plasma densities produced in higher ionization potential media. The results that we present might hence be a first valuable guide for future experiments. In our simulations, we use the soft-Coulomb potential

$$V(x) = -\frac{1}{\sqrt{x^2+\beta^2}}, \tag{1}$$

where we use atomic units and $\beta^2 = 0.0252$. The IR field is a 800-nm wavelength, 4-fs $\sin^2$ pulse with a peak intensity of 2.5×10^{15} W/cm^2, which produces a maximum of $\approx$0.2% ground-state depletion. The seed XUV–x-ray pulse is a $\sin^2$ pulse with a peak intensity of 2.5×10^{11} W/cm^2 and a duration of 200 as. IXPA processes are sensitive to the different parameters involved in the interaction process, such as the intensity of the IR pulse and the associated ground-state depletion, as well as the duration and the frequency content of the weak XUV–x-ray attosecond pulse. In what follows we study the influence of the XUV–x-ray central photon energy together with the delay with respect to the IR pulse on the IXPA effect at the single-atom level.

Figure 1 shows a basic scheme for IXPA processes. The low-frequency region of the XUV–x-ray weak pulse is absorbed by the electron, a first step that is assisted by the presence of the strong IR driving pulse that modifies the Coulomb potential of the ion; in a second step the electron is accelerated in the continuum by the IR electric field, reaching the necessary energy at the correct time so that a higher-frequency region of the XUV–x-ray pulse, optimally the central frequency region, stimulates the emission in a third step. The process is produced in the time scale of the duration of the XUV–x-ray pulse and benefits from the reshaping (chirp) during the interaction with the medium, as will be further detailed below.

In order to describe IXPA processes it is useful to compute the XUV–x-ray probe absorption spectrum, as described in [22], which represents the absorption of a weak probe pulse following a nonlinear excitation by one or more *pump* laser pulses

$$S(\omega) \propto \mathrm{Im}[E_X^*(\omega)D_X(\omega)]. \tag{2}$$

To probe the state of our system due to the nonlinear excitation caused by the presence of both the strong IR field and the

*carles.serrat-jurado@upc.edu

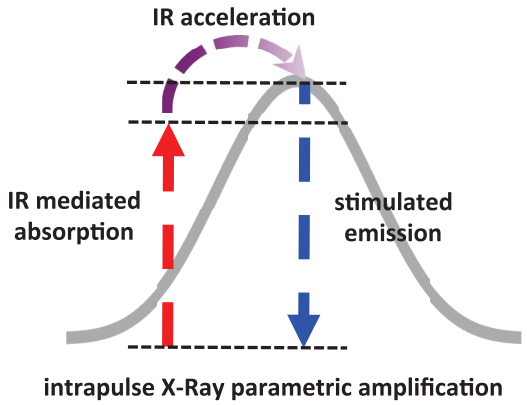

FIG. 1. Schematic of a strong-field-mediated IXPA.

weak XUV–x-ray pulse, we remove from the time-dependent dipole acceleration obtained in the TDSE integration the response of the system to the IR field alone and hence purely HHG processes are not included in the time-dependent dipole acceleration that plays the role of the pump in Eq. (2). We therefore define $D_X(\omega) = D(\omega) - D_{\rm IR}(\omega)$, where $D(\omega)$ is the complete spectrum obtained from the excitation of the system and $D_{\rm IR}(\omega)$ is the spectrum corresponding to the excitation of the system with the IR field alone. In this way, $S(\omega)$ calculates the absorption that a weak probe pulse $E_X^*(\omega)$ would experience interacting with a system that has been pumped and presents the time-dependent dipole acceleration that gives the spectrum $D_X(\omega)$, which includes the linear response to the weak XUV–x-ray pulse. The probe pulse $E_X^*(\omega)$ in our calculations is the seed that we consider for the combined IR plus XUV–x-ray interaction.

Figure 2 shows the probe absorption spectra for the case of a 113-eV XUV pulse interacting with the ion together with the

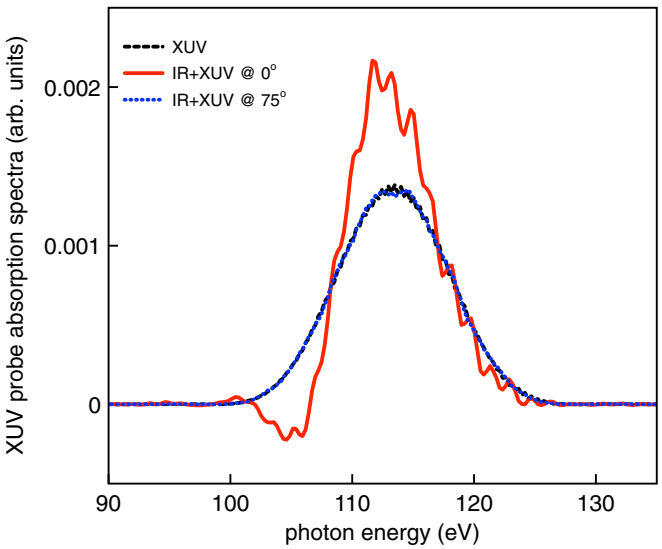

FIG. 2. XUV–x-ray probe absorption spectrum for a 113-eV XUV pulse interacting together with the IR pulse at a delay of 0° (red solid line), and 75° (blue dotted line), as indicated. The black dashed line shows the probe absorption spectrum in the case that the XUV pulse interacts alone with the ion.

IR pulse at two different delays. The red curve shows the case that the XUV pulse and the IR pulse are synchronized at a delay of 0° and the blue dotted curve shows the case for which the delay is equal to 75°. The results are compared to the case for which the weak XUV pulse interacts alone with the ion (black dashed curve), which gives a purely linear response. From the calculated probe absorption spectra (Fig. 2), it is clear that only certain delays between the IR and the XUV pulses can produce an effect different from the linear response. The red curve at a delay of 0° shows probe emission (negative values) at the lower frequencies of the XUV pulse, around 105 eV, which means that the probe pulse finds the system in an excited state, producing stimulated emission and hence probe gain at this frequency range. The red curve in Fig. 2 also shows probe absorption (positive values) around the central frequency of the XUV pulse that overcomes the probe absorption calculated for the purely linear case (black line), which means that the stimulated emission produced in this region by the IXPA process has depleted the excited state as compared to the linear case and therefore the probe absorption is higher. Indeed, the probe absorption spectral shape shown by the red line in Fig. 2 is a signature of an intrapulse parametric process.

For a full characterization of the parametric processes we use two more tools. (i) We compare the spectra from the response of the system to the IR pulse alone, the XUV–x-ray pulse alone, and the combined IR plus XUV–x-ray pulses considering different delays between them. (ii) We perform a frequency-time analysis to determine at which times the signals are emitted. Furthermore, in the frequency-time analysis, we identify the IR-driven stimulated emission and absorption processes by removing the contributions from the signal produced by the IR pulse alone and the one produced by the XUV–x-ray pulse alone. As it will be further discussed below, this analysis allows us to determine the parameter regions where IR-driven parametric amplification in the spectral range of the seeded XUV–x-ray pulse occurs.

First, in order to determine the parameter ranges where nonlinear stimulated absorption occurs, we have calculated the integral of the negative regions of the XUV–x-ray probe absorption spectrum by varying both the XUV–x-ray central photon energy from 90 eV to 400 eV and the delay between the XUV–x-ray pulse and the IR field between $-180°$ and 180°. The resulting map (Fig. 3) illustrates where the IXPA processes most probably arise, since nonlinear stimulated absorption is a necessary step to produce them. Note that Fig. 3 nicely reproduces the shape of the IR electric field as it was already observed in [14]. The particular cases shown in Fig. 2 hence correspond to the 113-eV photon energy value in Fig. 3 at the delays 0° and 75°.

Figure 4 shows the output spectra obtained for the particular case shown in Fig. 2 around 113 eV. The black dashed line in Fig. 4 corresponds to the spectrum obtained with only the strong IR pulse and the blue dotted line is the spectrum obtained with only the 113-eV XUV pulse. We note that the HHG yield produced by the Li^+ ion is about four orders of magnitude less than the linear response of the ion to the XUV pulse alone. The red line in Fig. 4 shows the spectrum obtained when both the XUV and IR pulses are sent together and synchronized at a delay of 0°. We can see that the spectral shape nicely follows the characteristics of an IXPA process,

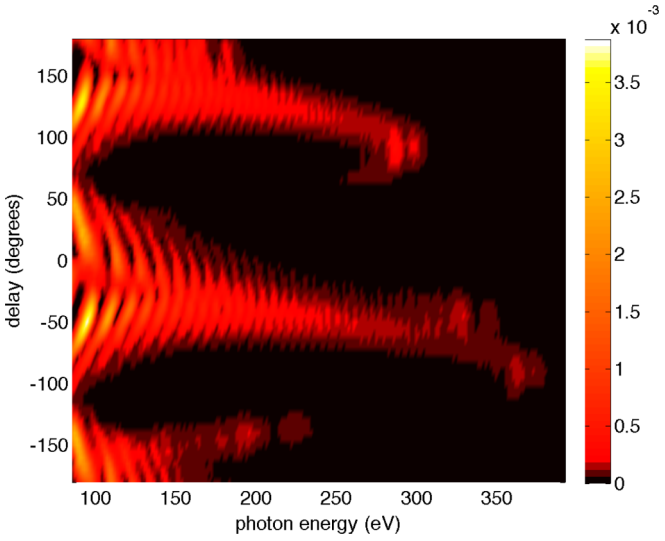

FIG. 3. Integrated negative regions of the XUV–x-ray probe absorption spectra as a function of the central photon energy of the XUV–x-ray pulse and the delay between the IR and XUV–x-ray pulse.

as it was also determined by the probe absorption spectrum in Fig. 2. We observe the absorption of the energy around 105 eV and also the amplification of the signal beyond the linear response about the central frequency of the XUV pulse. When the XUV pulse is not optimally synchronized with the IR pulse, however, the nonlinear effects disappear and we obtain basically the same probe absorption spectrum (blue line in Fig. 2) and output spectrum (green line in Fig. 4) that are obtained by considering the interaction with the XUV pulse alone.

Figure 5 shows the frequency-time analysis of some of the spectra calculated by considering the results in Fig. 3. Figures 5(a) and 5(b) show the spectra at 113 eV for a delay of 0° and Figs. 5(c) and 5(d) correspond to the higher

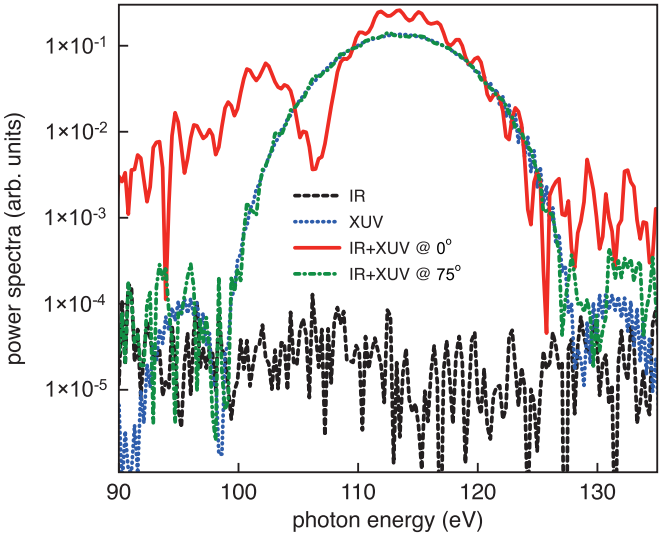

FIG. 4. Output spectra obtained from the Fourier transform of the time-dependent dipole acceleration, around the 113-eV region and for four different interaction cases, as indicated.

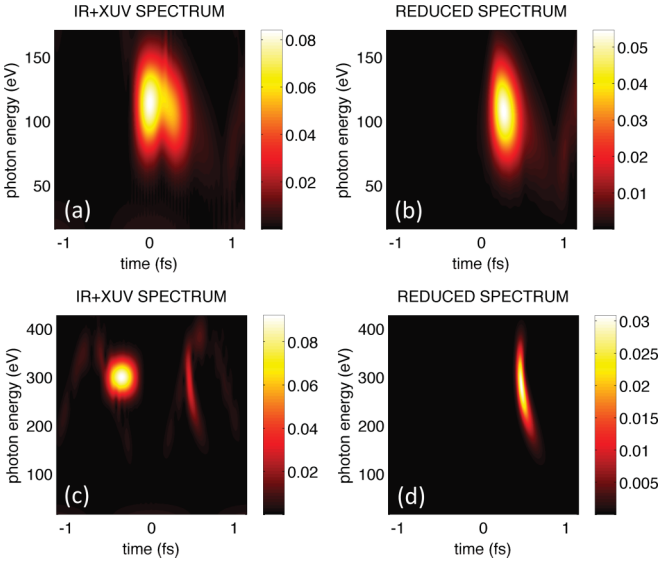

FIG. 5. Frequency-time analysis. (a) and (b) Spectra around 113 eV for a delay of 0°. (c) and (d) Spectra around 300 eV for a delay of −50°. The reduced spectra in (b) and (d) are obtained by subtracting the response of the IR pulse alone and the one of the XUV pulse alone from the total spectra, as explained in the text.

photon energy of 300 eV and for a delay of −50°. Both cases correspond to areas in Fig. 3 where IXPA is expected to occur. Figure 5(a) shows the frequency-time spectra for the full IR plus XUV response around the 113-eV spectral region. In this figure we can observe both the effect of the linear response at the position where the XUV has been added, i.e., at a delay of 0° ($t = 0$), and the nonlinear response around $t \approx 0.2$ fs. As already commented above, it is worth noting that the 200-as XUV pulse is chirped due to dispersion during the interaction with the ion and consequently time broadened, which allows the IXPA processes to be produced at $t \approx 0.2$ fs in this case. In Fig. 5(b) we plot the spectrum resulting from removing from the total response the one due to the IR pulse alone and the one due to the XUV pulse alone so that we remove the pure HHG contribution and the contribution of the linear response of the medium to the XUV pulse. We call it the reduced spectrum in Figs. 5(b) and 5(d) and hence it only shows the nonlinear contribution due to the combination of IR and XUV–x-ray assisted effects. We note that the amplified signal [Fig. 5(b)] is slightly down chirped. A similar behavior is shown in Figs. 5(c) and 5(d) by considering a higher-photon-energy x-ray seed pulse of 300-eV central photon energy. In this case the optimal delay, as calculated in Fig. 3, is about −50° ($t \approx -0.4$ fs). The nonlinear amplified IXPA signal is produced in this case at $t \approx 0.5$ fs, which again shows that the initial transform-limited x-ray seed is time broadened during the interaction with the Li^+ ion.

Finally, we address the effect of the added XUV–x-ray pulse (by taking as an example the 113 eV seed pulse) on the larger photon energy regions of the HHG spectrum. As shown in Fig. 6, a considerable increase of the HHG yield is obtained in the case of adding a seed pulse at 113 eV, with a plateau of harmonics that ends in this case at about 400 eV. We observe that this enhancement of the HHG yield depends

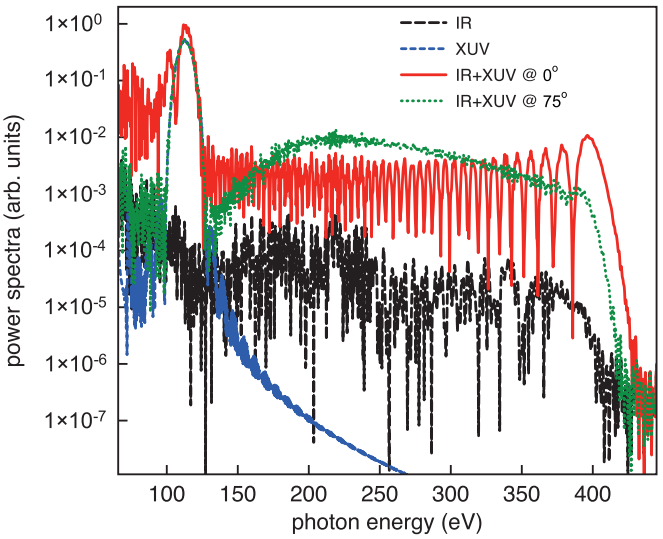

FIG. 6. Spectra obtained from the Fourier transform of the time-dependent dipole acceleration for the spectral region between 90 and 450 eV for four different interaction cases, as indicated.

on the delay between the XUV and the IR pulse, as it is clear from Fig. 6. Indeed, the red line in Fig. 6 shows spectrally separated harmonics and corresponds to a delay of 0°, while the green line corresponds to a delay of 75° and shows a basically flat plateau. This behavior clearly corresponds to enhanced ionization phenomena that have been extensively studied [23–25]. Importantly, although it is not the central subject of this paper, we observe that the enhanced ionization effect is highly robust for the parameter ranges that have been here considered.

We have hence demonstrated IXPA processes in high-order harmonic generation at the single-atom level by using *ab initio* simulations and have determined optimal parameter ranges for IXPA processes to occur. Our study corroborates previous theoretical work performed under the SFA [11,13,14]. We conclude that several parameters are decisive and need to be balanced for IXPA processes to arise, such as the peak intensity of the driving IR pulse, the ionization potential of the medium, and the duration and spectral contents of the weak XUV–x-ray seed pulses. As already clear from previous studies, the delay between the weak seed and strong driving pulses is crucial for the amplification. The avalanche effects expected from IXPA processes when propagation and macroscopic effects are considered [14] result in exponential growth of the XUV–x-ray signal, which might be of importance for the implementation of intense tabletop XUV–x-ray lasers and also used as spectral narrow seeds for fully coherent plasma x-ray amplifiers.

Financial support from the Spanish Ministry of Economy and Competitiveness (FIS2014-51997-R) is acknowledged.

[1] P. Agostini and L. F. DiMauro, Rep. Prog. Phys. **67**, 813 (2004).
[2] T. Popmintchev, M.-C. Chen, D. Popmintchev, P. Arpin, S. Brown, S. Alisauskas, G. Andriukaitis, T. Balciunas, O. D. Mücke, A. Pugzlys, A. Baltuska, B. Shim, S. E. Schrauth, A. Gaeta, C. Hernández-García, L. Plaja, A. Becker, A. Jaron-Becker, M. M. Murnane, and H. C. Kapteyn, Science **336**, 1287 (2012).
[3] C. Serrat and J. Biegert, Phys. Rev. Lett. **104**, 073901 (2010).
[4] E. J. Takahashi, P. Lan, O. D. Mücke, Y. Nabekawa, and K. Midorikawa, Nat. Commun. **4**, 2691 (2013).
[5] F. Brizuela, C. M. Heyl, P. Rudawski, D. Kroon, L. Rading, J. M. Dahlstrom, J. Mauritsson, P. Johnsson, C. L. Arnold, and A. L'Huillier, Sci. Rep. **3**, 1410 (2013).
[6] S. Haessler, T. Balciunas, G. Fan, G. Andriukaitis, A. Pugzlys, A. Baltuska, T. Witting, R. Squibb, A. Zair, J. W. G. Tisch, J. P. Marangos, and L. E. Chipperfield, Phys. Rev. X **4**, 021028 (2014).
[7] C. Jin, G. Wang, H. Wei, A.-T. Le, and C. D. Lin, Nat. Commun. **5**, 4003 (2014).
[8] L. V. Dao, Kh. B. Dinh, and P. Hannaford, Nat. Commun. **6**, 7175 (2015).
[9] J. Seres, E. Seres, D. Hochhaus, B. Ecker, D. Zimmer, V. Bagnoud, T. Kuehl, and C. Spielmann, Nat. Phys. **6**, 455 (2010).
[10] J. Seres, E. Seres, and C. Spielmann, Phys. Rev. A **86**, 013822 (2012).
[11] C. Serrat, Phys. Rev. Lett. **111**, 133902 (2013).
[12] J. Seres, E. Seres, B. Landgraf, B. Ecker, B. Aurand, T. Kuehl, and C. Spielmann, Sci. Rep. **4**, 4234 (2014).
[13] C. Serrat, D. Roca, and J. Seres, Opt. Express **23**, 4867 (2015).
[14] C. Serrat, D. Roca, J. M. Budesca, J. Seres, E. Seres, B. Aurand, A. Hoffmann, S. Namba, T. Kuehl, and C. Spielmann, Opt. Express **24**, 8028 (2016).
[15] T. Bredtmann, S. Chelkowski, A. D. Bandrauk, and M. Ivanov, Phys. Rev. A **93**, 021402(R) (2016).
[16] C. Serrat, Appl. Sci. **2**, 816 (2012).
[17] C. Serrat, Phys. Rev. A **87**, 013825 (2013).
[18] M. Lewenstein, P. Balcou, M. Y. Ivanov, A. L'Huillier, and P. B. Corkum, Phys. Rev. A **49**, 2117 (1994).
[19] G. N. Gibson and J. Biegert, Phys. Rev. A **78**, 033423 (2008).
[20] E. Hijano, C. Serrat, G. N. Gibson, and J. Biegert, Phys. Rev. A **81**, 041401(R) (2010).
[21] E. Hijano, C. Serrat, G. N. Gibson, C. Figueira de Morisso Faria, and J. Biegert, J. Mod. Opt. **58**, 1166 (2011).
[22] S. Mukamel, in *Principles of Nonlinear Optical Spectroscopy* (Oxford University Press, Oxford, 1995), p. 103.
[23] A. D. Bandrauk and N. H. Shon, Phys. Rev. A **66**, 031401(R) (2002).
[24] J. Biegert, A. Heinrich, C. P. Hauri, W. Kornelis, P. Schlup, M. P. Anscombe, M. B. Gaarde, K. J. Schafer, and U. Keller, J. Mod. Opt. **53**, 87 (2006).
[25] M. Tudorovskaya and M. Lein, J. Mod. Opt. **61**, 845 (2014).